Journal of Solid State Chemistry 183 (2010) 2951–2956

Contents lists available at ScienceDirect

Journal of Solid State Chemistry

journal homepage: www.elsevier.com/locate/jssc

Influence of CO_2 activation on hydrogen storage behaviors of platinum-loaded activated carbon nanotubes

Seul-Yi Lee, Soo-Jin Park *

Department of Chemistry, Inha University, 253, Nam-gu, Incheon 402-751, South Korea

ARTICLE INFO

Article history:
Received 4 June 2010
Received in revised form
23 August 2010
Accepted 30 August 2010

Keywords:
Hydrogen storage
Multi-walled carbon nanotubes
Physical activation
Spillover effect
Platinum particle

ABSTRACT

In this work, platinum (Pt) metal loaded activated multi-walled carbon nanotubes (MWNTs) were prepared with different structural characteristics for hydrogen storage applications. The process was conducted by a gas phase CO_2 activation method at 1200 °C as a function of the CO_2 flow time. Pt-loaded activated MWNTs were also formulated to investigate the hydrogen storage characteristics. The microstructures of the Pt-loaded activated MWNTs were characterized by XRD and TEM measurements. The textural properties of the samples were analyzed using N_2 adsorption isotherms at 77 K. The BET, D–R, and BJH equations were used to observe the specific surface areas and the micropore and mesopore structures. The hydrogen storage capacity of the Pt-loaded activated MWNTs was measured at 298 K at a pressure of 100 bar. The hydrogen storage capacity was increased with CO_2 flow time. It was found that the micropore volume of the activated MWNTs plays a key role in the hydrogen storage capacity.

1. Introduction

Hydrogen is one of the ideal energy carriers instead of conventional fossil fuels, because of its cleanness and high energy density. It is crucial to find a suitable method for efficient hydrogen storage in order to utilize hydrogen in mobile applications [1]. Various storage methods have been extensively investigated, including liquid hydrogen, metal hydrides, electrosorption, high-pressure hydrogen, and physisorption in porous materials [2,3]. In recent years, among them, porous or nanostructural carbon materials have been considerable experimental and theoretical interests in the use of adsorbents due to their potential for hydrogen storage via physisorption, which also have the advantages of its reversible storage reaction and safety [4–6].

In particular, carbon nano-materials (such as nanotubes and nanofibers) have attracted attention as one of potential adsorbents for hydrogen storage. Dillon et al. [7] first found that single-walled carbon nanotubes (SWNTs) have significant hydrogen storage capacities with 5–10 wt%. Also, Chambers et al. [8] claimed that the graphite nanofibers could adsorb hydrogen up to 67 wt% at 300 K/100 atm. However, these hydrogen storage capacities had not been successfully reproduced by any other groups. In recent publications [9–11], almost all experimental results indicated that hydrogen storage by carbon nano-materials was only 0.1–2.0 wt%.

Carbon nanotubes (CNTs) have become one of the most interesting materials due to their novel structure characteristics that include their nanometer hollow tubes, high surface area with a narrow pore distribution size, and low mass density. Particularly, their high surface area is very important in hydrogen storage applications, because materials with larger specific surface areas can commonly store more hydrogen [12]. Multi-walled carbon nanotubes (MWNTs) can be regarded as prospective reversible hydrogen storage media; however, their specific surface area is not very large (the typical value is approximately 200 m^2/g), which hinders the application of MWNTs as hydrogen storage materials. Currently, a considerable amount of attention has been focused not only on increasing the extended surface area, but also on developing micro porosity in MWNTs to obtain high-capacity hydrogen storage via various activation methods [13–17]. The porosity enhancement of MWNTs after physical activation is suggested as a means of opening the ends of MWNTs, and enhancing the defective cavities on the surface; this influences the hydrogen storage capacities through an increase in the number of activated MWNTs that in turn stems from the altered surface characteristics after the MWNT enhancement [18,19].

Furthermore, many researchers have investigated the hydrogen storage performance of carbon materials decorated with alkali metals, such as Li [20] and transition metals such as Pt, Pd, Ni, and Ti [21–23]. The function of the transition metal is to dissociate hydrogen molecules into protons or atoms, so that the

* Corresponding author. Fax: +82 32 860 8438.
E-mail address: sjpark@inha.ac.kr (S.-J. Park).

0022-4596/$ - see front matter © 2010 Elsevier Inc. All rights reserved.
doi:10.1016/j.jssc.2010.08.035

hydrogen can easily penetrate into the interlayers and defects of the carbon materials. In particular, activated MWNTs with a high specific surface area or a defective structure tend to exhibit high hydrogen storage capacities, with a hydrogen spillover effect; hence, hydrogen spillover is a viable approach in the enhancement of hydrogen storage [22,24].

In the present study, activated MWNTs loaded by platinum (Pt) metal were investigated in terms of their capability to enhance the hydrogen storage capacity with the CO_2 flow time. As activated MWNTs are considered to be the most promising material for practical applications of hydrogen storage, the textural properties of physically activated MWNTs were correlated to the hydrogen adsorption capacities to determine the factors that can improve the design of carbon-based hydrogen adsorbents.

2. Materials and methods

2.1. Materials and sample preparation

Commercially available multi-walled carbon nanotubes (MWNTs, purchased from the Nano Solution Co. Ltd. (Korea)), with a purity rating of ~90%, produced by chemical vapor deposition were used in this study. The diameter and length of the MWNTs were 10–25 nm and 20–50 μm, respectively. And, the specific surface area and total pore volume of the crude MWNTs were 185 m^2/g and 0.505 cm^3/g, respectively.

A physical activation process in a CO_2 gas atmosphere was performed to modify the material characteristics of the MWNTs as a function of the CO_2 flow time, and the activation temperature was fixed at 1200 °C. The MWNT samples were placed in a tube furnace, which was set to a heating rate of 2 °C/min with temperatures rising to 1200 °C under an N_2 flow. The temperature was maintained throughout the CO_2 gas flow at a flow rate of 50 cc/min (0, 10, 20, and 40 min). Pt particles were then introduced onto the activated MWNTs, prepared from the previous process, with a fixed Pt amount (5 wt% in the activated MWNTs). The loading of Pt particles was performed by means of a well-known chemical reduction method [25]. The activated MWNTs were suspended in an ethylene glycol (EG) solution. An EG solution containing chloroplatinic acid hexahydrate (H_2Cl_6Pt) was slowly added dropwise to this solution, and this was stirred mechanically for 4 h under an N_2 atmosphere. The 1.0 M NaOH solution was added to adjust the pH of the solution, and the solution was then heated to 120 °C for 2 h to completely reduce the Pt particles. The Pt-loaded activated MWNT samples were termed according to the function of the CO_2 gas flow time: Pt-Acti-0, Pt-Acti-10, Pt-Acti-20, and Pt-Acti-40.

2.2. Characterization

The X-ray diffraction (XRD) revealed the crystalline phase and lattice distortion changes of the Pt-loaded activated MWNTs. This also showed the presence of Pt particles on the MWNT surfaces. The XRD data of the samples were collected using a Rigaku model D/MAX diffractometer with Cu$K\alpha$ radiation (0.154 nm). The Raman spectra were observed using a Bruker model RFS 100/S with the excitation wavelength of a He–Ne laser of 600 nm, at a power of 500 mV. This showed the defects and growth in the tubes through comparisons of the D- and G-bands intensities. Transmission electron microscopy (TEM) was used for the observation of the Pt-loaded activated MWNTs. For the analysis, few milligrams of the samples were dispersed in anhydrous ethanol and a drop of this suspension was deposited onto a TEM grid covered by lacey amorphous carbon film. Also, the average particle size and particle size distribution were obtained from a few randomly chosen areas in the TEM image containing approximately 100 nanoparticles each. Porous textural characterizations of all samples were done by physical adsorption of an N_2 at 77 K, using a model ASAP 2020 device by Micromeritics Co., Ltd. The samples were degassed at 573 K for 12 h to obtain a residual pressure of less than 10^{-6} mmHg. Specific surface areas and the micropore volume of the samples were determined from Brunauer–Emmett–Teller (BET) equation and by Dubinin–Radushkevitch (D–R) equation, respectively. The amounts of an N_2 adsorbed at relative pressures ($P/P_0=0.98$) were used to investigate the total pore volumes, which corresponded to the sum of the micropore and mesopore volumes. Also, the micropore and mesopore size distributions of samples were calculated Horvath–Kawazoe (H–K) equation and Barrett–Joyner–Halenda (BJH) method, respectively. Atomic absorption spectrometry (AAS, AA-SCANI, Thermo Jarrell Ash Co.) was used to measure the Pt-loaded weight in the Pt-loaded activated MWNTs.

2.3. Hydrogen storage capacities

A hydrogen uptake experiment was conducted under an ambient condition of 298 K and both moderate and low pressure (100 bar) conditions, which are compatible with future electric-vehicle applications. In each experiment, approximately 0.5 g of the sample was loaded into a stainless chamber. Before the measurement, the system was evacuated for 3 h, and the sample chamber was heated to 398 K. After the chamber was cooled to room temperature, hydrogen was introduced until a pressure of 100 bar was attained. An ultra-high-purity grade (99.9999%) of hydrogen was used so that the influences of moisture and other impurities could be excluded. Finally, a volumetric measurement method was used to determine the hydrogen uptake capacities after degassing to remove storage hydrogen.

3. Results and discussion

3.1. Characterization

XRD patterns of the Pt-loaded activated MWNTs as a function of the CO_2 flow time are shown in Fig. 1. The diffraction peaks at $2\theta=26°$ and 54° correspond to the (0 0 2) and (0 0 4) reflection planes (interlayered spacing between adjacent graphite layers), respectively. Along with these diffractions, the reflection peaks of (1 0 0) and (1 0 1) corresponding to the in-plane orderings are

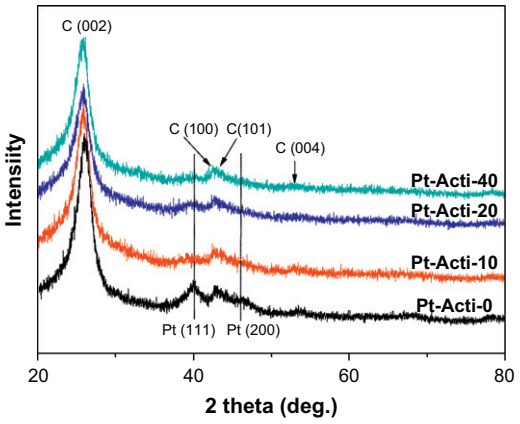

Fig. 1. XRD patterns of the Pt-loaded activated MWNTs, as a function of CO_2 flow time.

shown at $2\theta=42^\circ$ and 43.5°, respectively [26]. In addition, a sharp decrease in the intensity as well as a broadening of the (0 0 2) Bragg peak can be observed as the CO_2 flow time increases. The XRD analysis allowed an evaluation of the effect of the CO_2 flow time at 1200 °C on the interlayer spacing. As shown in Fig. 1, in spite of the CO_2 activation at high temperature, the d_{002} value increased slightly in the range of 3.412–3.454 Å. These results indicate that there is no significant effect of the CO_2 flow time on the graphitization degree of MWNTs. Additionally, the Pt particles on the MWNTs were confirmed from the respective X-ray diffractograms. It is known that pure-metallic Pt has a faced-centered cubic (fcc) structure [27,28]. The peaks at $2\theta=40^\circ$ and 47° can be characterized with the (1 1 1) and (2 0 0) planes, respectively. However, no Pt phase was detected owing to the absence of reflections at $2\theta=40^\circ$ and 47°, except for the Pt-Acti-0 sample. This can be attributed to the high dispersion of the Pt particles, as the relatively high dispersion of metals at low loadings would be one reason for the absence of the XRD peaks from the metals, as suggested in earlier studies [29,30]. Thus, it was found that the enhanced surface area of MWNTs has an effect on the loading and dispersion characteristics of Pt particles. It is important to note that Pt particles have been successfully loaded on activated MWNT surfaces, combining the result from the AAS analysis presented in Table 1.

Raman spectra of Pt-loaded activated MWNTs, as a function of the CO_2 flow time, are shown in Fig. 2. This represents an important tool to provide an information about the crystal structure and the presence of disorder in the MWNTs. The frequencies at around 1600 cm^{-1}, which correspond to the tangential C–C stretching vibration, known as the graphite mode G-band, were investigated; as were those around 1280 cm^{-1}, which are related to local defects that originate from structural imperfections in the MWNTs, known as the defect mode D-band. Measuring the ratio of the intensities of the D- and G-bands provides some idea of the disorder of the Pt-loaded activated MWNTs. As shown in Fig. 3, the I_D/I_G ratio of the Pt-loaded activated MWNTs increases as the CO_2 flow time to the Pt-Acti-20 increases, after which it decreases. This result clearly implies that the graphitic structure of the MWNTs became disordered after CO_2 activation. It is interesting that the ratio of I_D/I_G in Pt-Acti-40 is smaller than that in Pt-Acti-20, which may be attributed to the fact that the disordered structure of the external surface of Pt-Acti-40 decomposes at a higher temperature [31].

Fig. 4 shows TEM images of Pt-loaded activated MWNTs before and after the CO_2 activation step. Fig. 4(a) shows Pt-Acti-0, the average diameter of MWNTs being around 25 nm. Additionally, Fig. 4(b) shows Pt-Acti-20. It was found that the MWNTs experienced a decrease in the diameter to around 15 nm, and that they have a comparatively straight shape as a result of surface oxidation during the CO_2 activation process. Moreover the Pt particles were dispersed on the MWNTs with less relative uniformity compared to the Pt-Acti-0 sample. This result is in good agreement with that shown in Fig. 1, implying the formation of larger particles along with the low dispersion rate, with the comparable Pt content of all samples.

Fig. 5 shows the nitrogen isotherm of the Pt-loaded activated MWNTs as a function of the CO_2 flow time. This shows that the adsorption volume increased after the CO_2 activation process. It was clearly expected that the specific surface area and total pore volume of the Pt-loaded activated MWNTs were all enhanced after the CO_2 activation step. According to the IUPAC classification, the evolution of all samples on adsorption isotherms, as P/P_0 increases, can be described as a type-II isotherm with

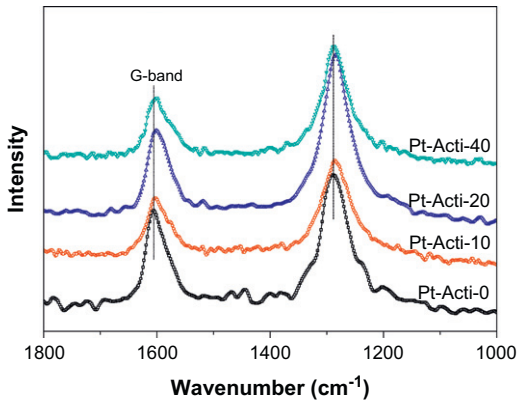

Fig. 2. Raman spectra of the Pt-loaded activated MWNTs, as a function of CO_2 flow time.

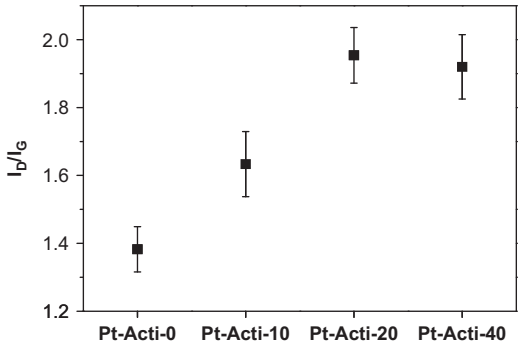

Fig. 3. Intensity ratio (I_D/I_G) of the Pt-loaded activated MWNTs, as a function of CO_2 flow time.

Table 1
Textural properties and Pt-loaded weight of Pt-loaded activated MWNTs, as a function of CO_2 flow time.

Specimens	C_{BET}[a]	E_n (kJ/mol)[b]	S_{BET} (m^2/g)[c]	V_{Total} (cm^3/g)[d]	V_{Micro} (cm^3/g)[e]	V_{Meso} (cm^3/g)[f]	F_{Micro} (%)[g]	F_{Meso} (%)[h]	Pt content (wt%)
Pt-Acti-0	32	2.218	207	0.559	0.063	0.496	11.3	88.7	2.2
Pt-Acti-10	58	2.600	347	0.897	0.115	0.782	12.8	87.2	3.3
Pt-Acti-20	70	2.719	333	0.691	0.120	0.572	17.2	82.8	3.1
Pt-Acti-40	43	2.408	275	0.589	0.088	0.501	14.9	85.1	2.4

[a] C_{BET}: BET constant $C=(a_1\upsilon_2)/(a_2\upsilon_1)\ e^{(q1-qL)RT}$.
[b] E_n: net heat of adsorption energy, $\Delta E=q_1-q_L=RT\ln(C)$ $(a_1\upsilon_2=a_2\upsilon_1)$.
[c] S_{BET}: specific surface area calculated, using BET equation at a relative pressure range 0.2–0.35.
[d] V_{Total}: total pore volume is estimated at a relative pressure $P/P_0=0.98$.
[e] V_{Micro}: micropore volume determined from Dubinin–Radushkevic equation.
[f] V_{Meso}: mesopore volume determined from the subtraction of micropore volume from total pore volume.
[g] F_{Micro}: fraction of micropore volume=(micropore volume/total pore volume) × 100.
[h] F_{Meso}: fraction of mesopore volume=(mesopore volume/total pore volume) × 100.

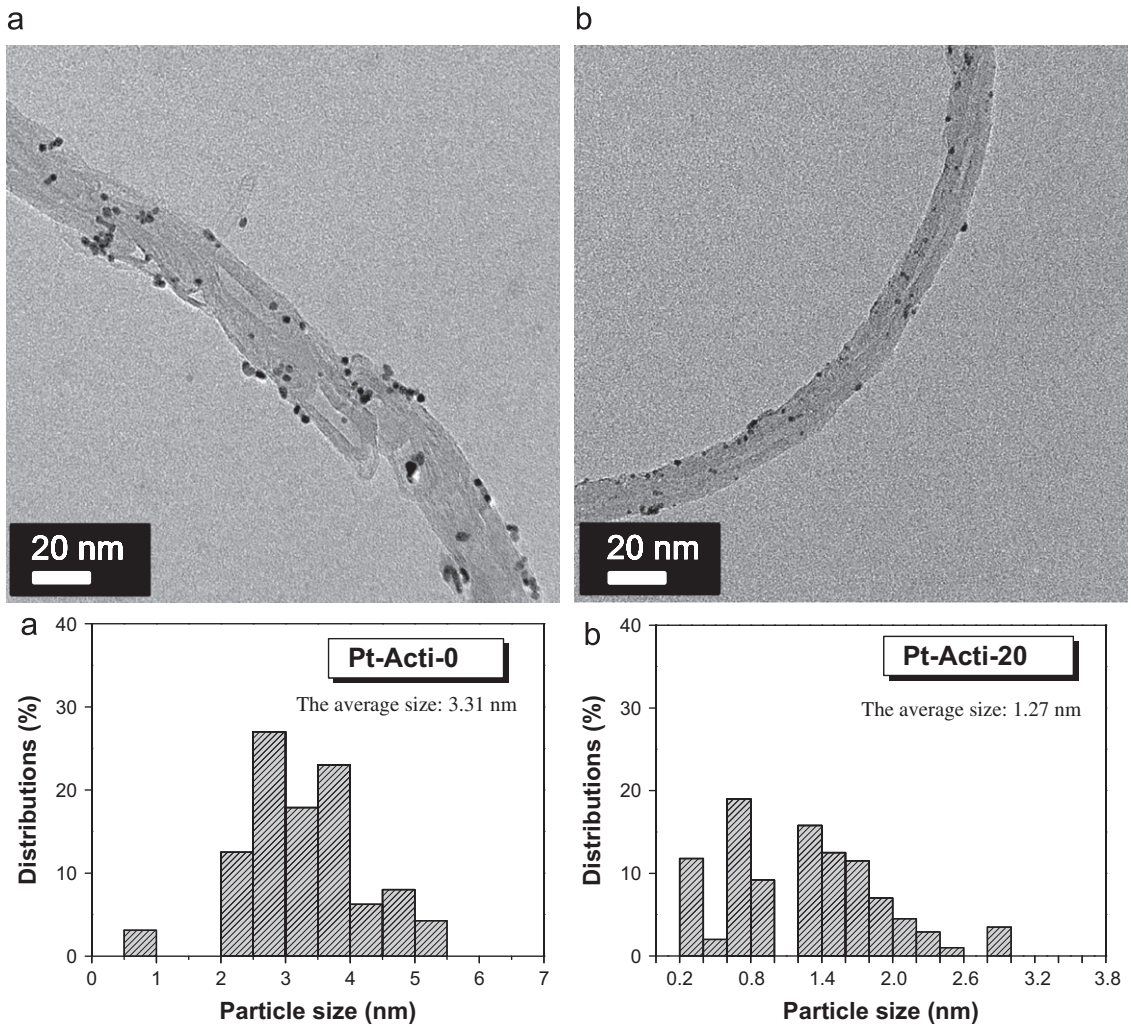

Fig. 4. TEM images and Pt particle size distributions of the Pt-Acti-0 (a) and Pt-Acti-20 (b).

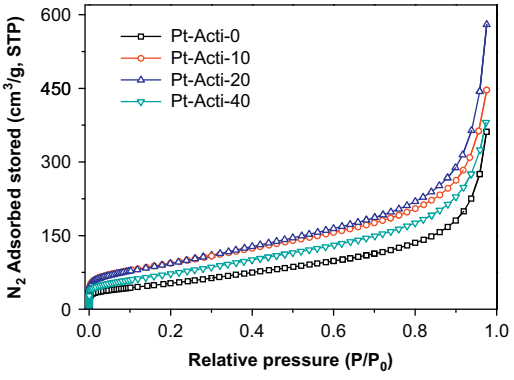

Fig. 5. Nitrogen adsorption isotherms of the Pt-loaded activated MWNTs, as a function of CO_2 flow time.

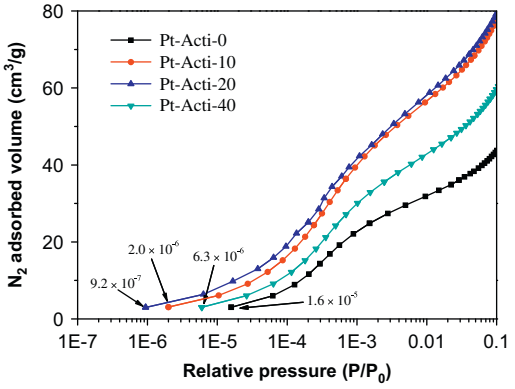

Fig. 6. Nitrogen adsorption isotherms in the logarithmic pressure scale of the Pt-loaded activated MWNTs, as a function of CO_2 flow time.

a characteristic H1 hysteresis. The H1 hysteresis observed above $P/P_0=0.6$ is attributed to the capillary condensation that normally results from the intertubular structure of the samples, which is also indicative of cylindrically shaped pores. The specific surface areas of the MWNTs are estimated from the linear fit to the BET adsorption isotherms for the relative pressure range of P/P_0 0.2–0.35.

Fig. 6 shows the nitrogen adsorption isotherms in the logarithmic pressure scale at low relative pressure of the Pt-loaded activated MWNTs, as a function of CO_2 flow time. It is found that the nitrogen adsorption of the samples after CO_2 activation is initiated at lower relative pressure in comparison with Pt-Acti-0 sample. In the Pt-Acti-20 sample, this phenomenon is remarkably revealed in the 9.2×10^{-7} of relative pressure, which indicates that the micropores in that relative pressure predominated.

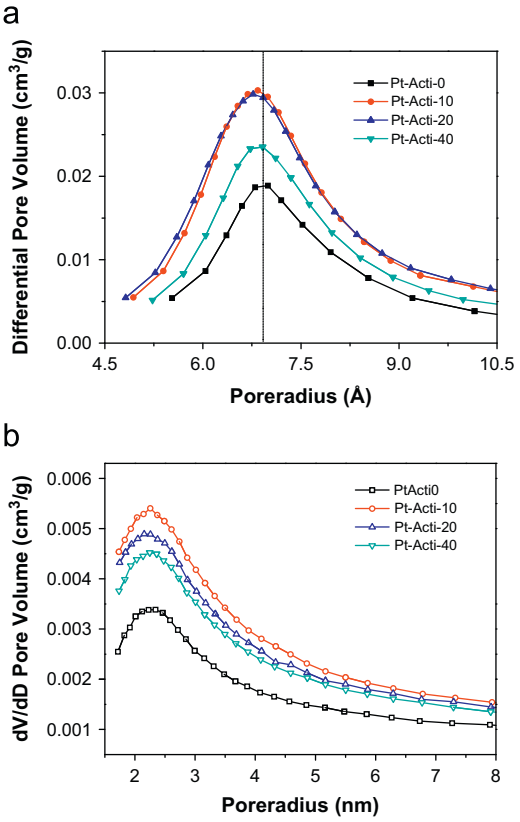

Fig. 7. Micropore (a) and mesopore (b) size distribution of the Pt-loaded activated MWNTs, as a function of CO_2 flow time.

To understand the pore structures of the samples in detail, Table 1 lists the textural properties as a function of the CO_2 flow time. The Pt-Acti-10 sample has the highest specific surface area and total pore volume values of 347 m^2/g and 0.897 cm^3/g. However, it is interesting to note that the micropore volume fraction of the Pt-Acti-20 sample shows the highest value. This can be attributable to the fact that the CO_2 activation process transforms some of the mesopores into micropores. According to the literature [32], CO_2 activation can produce surface functional groups that can attach to the pore walls, resulting in a shrinking of the pore width. However, excess CO_2 activation causes a decrease in the specific surface area and pore volume, as the MWNTs may be thinned and numerous defects on their surfaces can collapse. This result is related to the micro- and mesopore size distribution of the samples, as shown in Fig. 7. It was found that the pore volume of all of the activated MWNTs increased after the CO_2 activation process, as expected [33]. Moreover it was observed that the micropore size distribution in both the Pt-Acti-10 and Pt-Acti-20 samples shifted to the left side. From these two samples, the pore size of the Pt-Acti-20 sample becomes smaller than that of the Pt-Acti-10 sample.

3.2. Hydrogen uptake capacities

Fig. 8 shows the hydrogen storage capacity values of the Pt-loaded activated MWNTs, as a function of the CO_2 flow time. The hydrogen storage capacity of the samples increases with the activation time up to 20 min and then decreases, which has the highest hydrogen storage capacity of 0.41 wt% in the Pt-1200-20 sample. The same trend can be found for both the BET constant *C* and the net heat of adsorption energy. The BET constant can be strongly enhanced by increasing the micropore fraction [16]. For

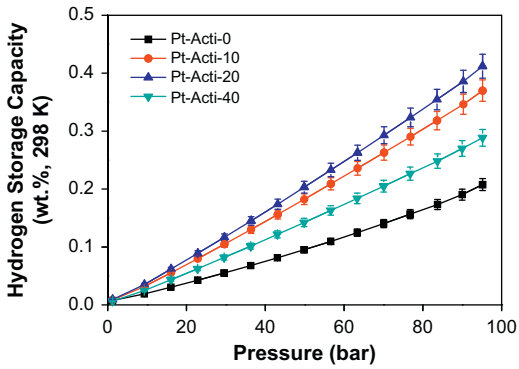

Fig. 8. Hydrogen storage capacities of the Pt-loaded activated MWNTs, as a function of CO_2 flow time.

this reason, the increase in the *C* value can correspond to the development of micropores of MWNTs, which is irrelevant to the characteristics of the specific surface area. In turn, the micropore fraction also influences the net heat of adsorption energy. Hence, the structural characteristics (defects on the external surface) of the activated MWNTs clearly affect the net heat of adsorption in the Pt-loading system on the activated MWNT surfaces, resulting in an improvement of the hydrogen storage capacity.

Normally, gas adsorption depends strongly on the micropores in the carbon nano-materials. The results of this study correspond with those of an earlier report [34–36]. From the results, it is concluded that the actual order of the hydrogen storage capacity is highly, as is that of the micropore volume. It is suggested that the microporous cavities on the MWNT surfaces offer an attraction force for hydrogen molecules [37]. Therefore, the hydrogen storage capacity of the Pt-loaded activated MWNTs, under common operating conditions (298 K/100 bar), can be attributed to the micropore that exists within favorable sites in the defective surface. Moreover it is very interesting that the Pt-Acti-20 sample showed greater capacity compared to that of the Pt-Acti-10 sample, when the micropore volumes of the samples were in a similar range, resulting in a feasible pore size distribution for hydrogen storage, as shown in Fig. 7(a).

Many researchers have investigated with the carbon materials in presence of metal catalysts (Pt, Pd, Ni, and so on), for the purpose of increasing the hydrogen storage capacities, both experimentally and theoretically [22,23,38]. These metal particles play an important role in enhancing of the hydrogen adsorption by the affinity of the metal particles and hydrogen, afterwards metal dissociates the hydrogen molecules and spills them over the metal–carbon interfaces [39–41].

As shown in Fig. 4, it is found that the size of Pt particles is one of the critical factors affecting the hydrogen storage capacities. The average size and size distributions of Pt particles might be attributable to the morphological characteristics of MWNTs, indicating that the Pt particles of Pt-Acti-20 sample are loaded uniformly and smaller than the Pt-Acti-0 sample. It is suggested that the well-developed micropore structures of activated MWNTs have an influence on the great metal-loading properties for enhancing the hydrogen storage capacity by spill-over.

4. Conclusions

In this work, platinum (Pt) metal loaded activated multi-walled carbon nanotubes (MWNTs) with different structural characteristics were investigated for hydrogen storage. It was found that the textural properties of the activated MWNTs strongly influence the net heat of adsorption in the Pt-loading

system of activated MWNT surfaces. It was noted that the presence of the Pt influenced the enhancement of the hydrogen storage capacity in the case of a well-developed micropore structure of activated MWNTs, as a function of the CO_2 flow time. Consequently, activated MWNTs optimized by both the activation and the presence of the Pt are porous materials that are potentially suitable for use as a catalyst carrier. This can lead to important applications in field of hydrogen storage materials.

Acknowledgement

This research was supported by a grant from the Fundamental R&D Program for Core Technology of Materials, funded by the Ministry of Knowledge Economy, Republic of Korea.

References

[1] M. Rzepka, P. Lamp, J. Phys. Chem. B 102 (1998) 10894–10898.
[2] M. Fichtner, Adv. Eng. Mater. 7 (2005) 443–455.
[3] K.P. Rao, A. Govindaraj, C.N.R. Rao, J. Solid State Chem. 180 (2007) 3571–3575.
[4] L. Schlapbach, A. Züttel, Nature 414 (2001) 353–358.
[5] Y. Li, D. Zhao, Y. Wang, R. Xue, Z. Shen, X. Li, J. Int., Hydrogen Energy 32 (2006) 2513–2517.
[6] T. Takei, O. Houshito, Y. Yonesaki, N. Kumada, N. Kinomura, J. Solid State Chem. 180 (2007) 1180–1187.
[7] A.C. Dillon, K.M. Jones, T.A. Bekkedahl, C.H. Kiang, D.S. Bethune, M.J. Heben, Nature 386 (1997) 377–379.
[8] A. Chambers, C. Park, R.T.K. Baker, N.M. Rodriguez, J. Phys. Chem. B 102 (1998) 4253–4256.
[9] L. Zhou, Y. Zhou, Y. Sun, Int. J. Hydrogen Energy 29 (2004) 475.
[10] S.U. Rather, R. Zacharia, M. Naik, S.W. Hwang, A.R. Kim, K.S. Nahm, Int. J. Hydrogen Energy 33 (2008) 6710–6718.
[11] H.Z. Geng, T.H. Kim, S.C. Lim, H.K. Jeong, M.H. Jin, Y.W. Jo, Y.H. Lee, Int. J. Hydrogen Energy 35 (2010) 2073–2082.
[12] B.J. Kim, Y.S. Lee, S. J., Int. J. Hydrogen Energy 33 (2008) 2254–2259.
[13] Y. Liu, Z. Shen, K. Yokogawa, Mater. Res. Bull. 41 (2006) 1503–1512.
[14] Q. Jiang, M.Z. Qu, B.L. Zhang, Z.L. Yu, Carbon 40 (2002) 2743–2745.
[15] J.J. Niu, J.N. Wang, Solid State Sci. 10 (2008) 1189–1193.
[16] B.J. Kim, Y.S. Lee, S.J. Park, J. Colloid Interface Sci. 306 (2007) 454–458.
[17] H.Y. Tian, C.E. Buckley, S. Mulè, M. Paskevicius, B.B. Dhal, Nanotechnology 19 (2008) 475605–475611.
[18] C.H. Chen, C.C. Huang, Micropor. Mesopor. Mater. 109 (2008) 549–559.
[19] S.J. Park, S.Y. Lee, Carbon Lett. 10 (2009) 19–22.
[20] S. Banerjee, I.K. Puri, Nanotechnology 19 (2008) 155702.
[21] S.U. Rather, N. Mehraj-ud-din, R. Zacharia, S.W. Hwang, A.R. Kim, K.S. Nahm, Int. J. Hydrogen Energy 34 (2009) 961–966.
[22] M. Zieliński, R. Wojcieszak, S. Monteverdi, M. Mercy, M.M. Bettahar, Int. J. Hydrogen Energy 32 (2007) 1024–1032.
[23] A.J. Lachawiec Jr., G. Qi, R.T. Yang, Langmuir 21 (2005) 11418–11424.
[24] S.C. Mu, H.L. Tang, S.H. Qian, M. Pan, R.Z. Yuan, Carbon 44 (2006) 762–767.
[25] S. Kim, S.J. Park, Anal. Chim. Acta 619 (2008) 43–48.
[26] H. Cao, M. Zhu, Y. Li, J. Solid State Chem. 179 (2006) 1208–1213.
[27] E.S. Steigerwalt, G.A. Deluga, C.M. Lukehart, J. Phys. Chem. B 106 (2002) 760–766.
[28] C.T. Hsieh, Y.W. Chou, W.Y. Chen, J. Alloys Compd. 466 (2008) 233–240.
[29] Y. Li, R.T. Yang, Ind. Eng. Chem. Res. 46 (2007) 8277–8281.
[30] D. Cheng, X. Zhu, Y. Ben, F. He, L. Cui, C. Liu, Catal. Today 115 (2006) 205–210.
[31] C.H. Chen, C.C. Huang, Micropor. Mesopor. Mater. 112 (2008) 553–560.
[32] B.J. Kim, S.J. Park, Nanotechnology 17 (2006) 4395–4398.
[33] Y. Luo, Y. Heng, X. Dai, W. Chen, J. Li, J. Solid State Chem. 182 (2009) 2521–2525.
[34] J.L.C. Rowsell, E.C. Spencer, J. Eckert, J.A.K. Howard, O.M. Yaghi, Science 309 (2005) 1350–1354.
[35] H. Noguchi, A. Kondo, Y. Hattori, H. Kajiro, H. Kanoh, K. Kaneko, J. Phys. Chem. C 112 (2007) 248–254.
[36] J.B. María, L.C. Dolores, S.G. Fabián, C.A. Diego, L.S. Ángel, Micropor. Mesopor. Mater 112 (2008) 235–242.
[37] J.J. Purewal, H. Kabbour, J.J. Vajo, C.C. Ahn, B. Fultz, Nanotechnology 20 (2009) 204012–204017.
[38] C.I. Contescu, C.M. Brown, Y. Liu, V.V. Bhat, N.C. Gallego, J. Phys. Chem. C 113 (2009) 5886–5890.
[39] L. Wang, R.T. Yang, Energy Environ. Sci. 1 (2008) 268–279.
[40] B.J. Kim, Y.S. Lee, S.J. Park, Int. J. Hydrogen Energy 33 (2008) 4112–4115.
[41] A.D. Lueking, R.T. Yang, Appl. Catal. A Gen. 265 (2004) 259–268.